SINTEF
PROCEEDINGS
1

Selected papers from 10th International Conference on Computational Fluid Dynamics in the Oil & Gas, Metallurgical and Process Industries

Progress in Applied CFD

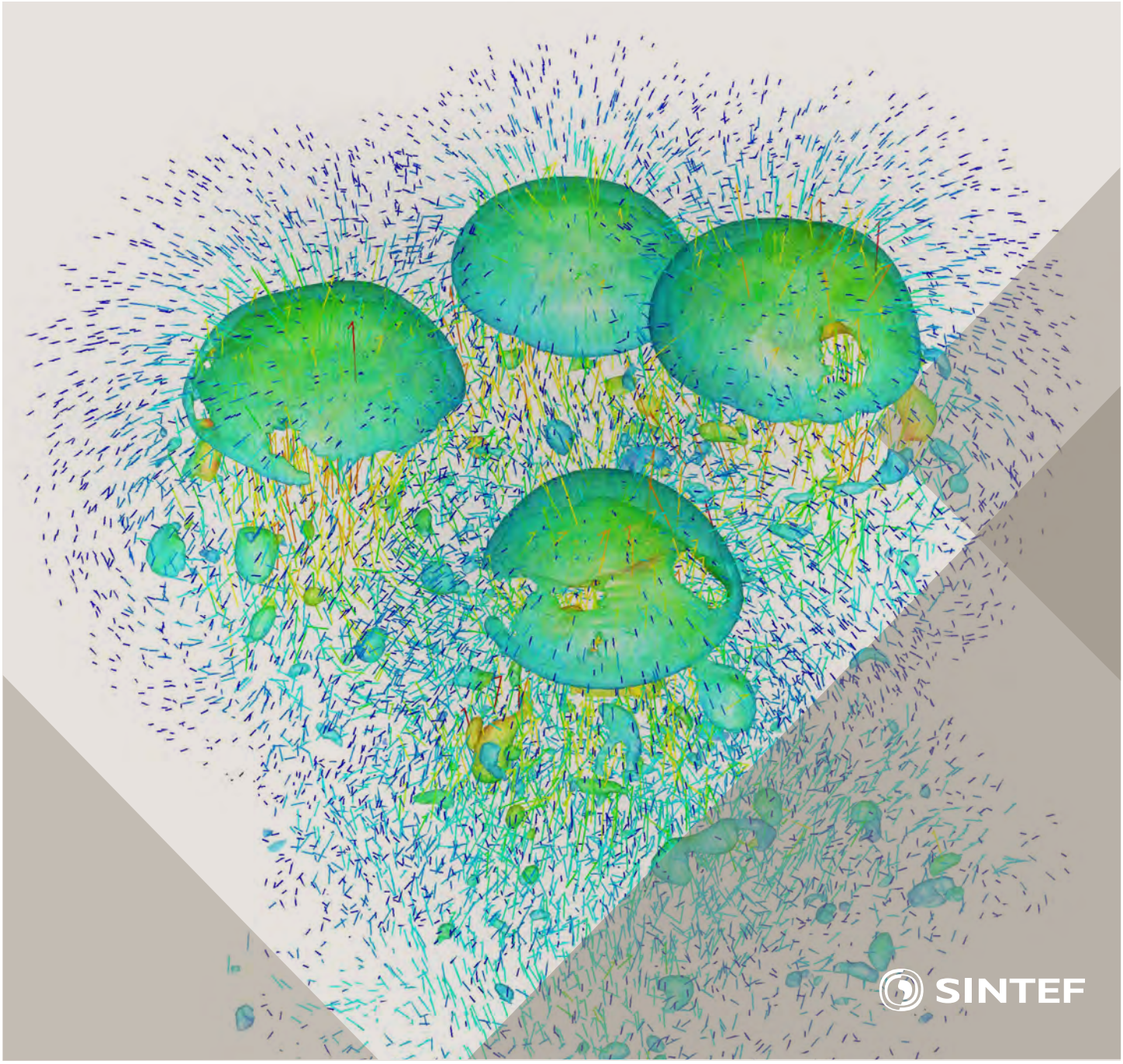

SINTEF Proceedings

Editors:
Jan Erik Olsen and Stein Tore Johansen

Progress in Applied CFD

Selected papers from 10th International Conference on Computational Fluid Dynamics in the Oil & Gas, Metallurgical and Process Industries

SINTEF Academic Press

SINTEF Proceedings no 1
Editors: Jan Erik Olsen and Stein Tore Johansen
Progress in Applied CFD
Selected papers from 10th International Conference on Computational Fluid Dynamics in the Oil & Gas, Metallurgical and Process Industries

Key words:
CFD, Flow, Modelling

Cover, illustration: Rising bubbles by Schalk Cloete

ISSN 2387-4287 (printed)
ISSN 2387-4295 (online)
ISBN 978-82-536-1432-8 (printed)
ISBN 978-82-536-1433-5 (pdf)

60 copies printed by AIT AS e-dit
Content: 100 g munken polar
Cover: 240 g trucard

SINTEF Academic Press
Address: Forskningsveien 3 B
PO Box 124 Blindern
N-0314 OSLO
Tel: +47 22 96 55 55
Fax: +47 22 96 55 08

www.sintef.no/byggforsk
www.sintefbok.no

SINTEF Proceedings
SINTEF Proceedings is a serial publication for peer-reviewed conference proceedings on a variety of scientific topics.
The processes of peer-reviewing of papers published in SINTEF Proceedings are administered by the conference organizers and proceedings editors. Detailed procedures will vary according to custom and practice in each scientific community.

PREFACE

This book contains selected papers from the 10th International Conference on Computational Fluid Dynamics in the Oil & Gas, Metallurgical and Process Industries. The conference was hosted by SINTEF in Trondheim in June 2014 and is also known as CFD2014 for short. The conference series was initiated by CSIRO and Phil Schwarz in 1997. So far the conference has been alternating between CSIRO in Melbourne and SINTEF in Trondheim. The conferences focus on the application of CFD in the oil and gas industries, metal production, mineral processing, power generation, chemicals and other process industries. The papers in the conference proceedings and this book demonstrate the current progress in applied CFD.

The conference papers undergo a review process involving two experts. Only papers accepted by the reviewers are presented in the conference proceedings. More than 100 papers were presented at the conference. Of these papers, 27 were chosen for this book and reviewed once more before being approved. These are well received papers fitting the scope of the book which has a slightly more focused scope than the conference. As many other good papers were presented at the conference, the interested reader is also encouraged to study the proceedings of the conference.

The organizing committee would like to thank everyone who has helped with paper review, those who promoted the conference and all authors who have submitted scientific contributions. We are also grateful for the support from the conference sponsors: FACE (the multiphase flow assurance centre), Total, ANSYS, CD-Adapco, Ascomp, Statoil and Elkem.

Stein Tore Johansen & Jan Erik Olsen

Organizing committee:

Conference chairman: Prof. Stein Tore Johansen
Conference coordinator: Dr. Jan Erik Olsen
Dr. Kristian Etienne Einarsrud
Dr. Shahriar Amini
Dr. Ernst Meese
Dr. Paal Skjetne
Dr. Martin Larsson
Dr. Peter Witt, CSIRO

Scientific committee:

J.A.M.Kuipers, TU Eindhoven
Olivier Simonin, IMFT/INP Toulouse
Akio Tomiyama, Kobe University
Sanjoy Banerjee, City College of New York
Phil Schwarz, CSIRO
Harald Laux, Osram
Josip Zoric, SINTEF
Jos Derksen, University of Aberdeen
Dieter Bothe, TU Darmstadt
Dmitry Eskin, Schlumberger
Djamel Lakehal, ASCOMP
Pär Jonsson, KTH
Ruben Shulkes, Statoil
Chris Thompson, Cranfield University
Jinghai Li, Chinese Academy of Science
Stefan Pirker, Johannes Kepler Univ.
Bernhard Müller, NTNU
Stein Tore Johansen, SINTEF
Markus Braun, ANSYS

CONTENTS

STATE OF THE ART IN MAPPING SCHEMES FOR DILUTE AND DENSE EULER-LAGRANGE SIMULATIONS

Stefan RADL,[1*] Begona C. GONZALES,[1] Christoph GONIVA,[2,3] Stefan PIRKER[3]

[1] Institute of Process and Particle Engineering, TU Graz, AUSTRIA

[2] DCS Computing GmbH, Linz, AUSTRIA

[3] Department of Particulate Flow Modelling, JKU Linz, AUSTRIA

* E-mail: radl@tugraz.at

ABSTRACT

Euler-Lagrange (EL) simulations are an extremely important tool for academia and industry to better understand gas-particle flows. We present simulation results for various gas-particle flow configurations using a variety of Lagrangian-to-Euler coupling schemes. Specifically, we have combined the idea of smoothing the exchange fields (as proposed by Pirker et al. (2011), as well as Capecelatro and Desjardins (2013)) to design a new generation of robust mapping schemes that allow implicit, explicit or a hybrid implicit/explicit time marching. Our schemes enable EL simulations of highly loaded gas-particle flows in which particles have a broad size distribution. We demonstrate the performance of our mapping schemes for the case of (i) a bubbling bi-disperse fluidized bed, (ii) a freely sedimenting suspension, as well as (iii) particle injection in turbulent cross flow configurations.

Keywords: Euler-Lagrange, numerical schemes, gas-particle flow.

NOMENCLATURE

Greek Symbols

β	Friction coefficient, [kg/m³/s]
ϕ	Mass density, [kg/m^3]
γ	Transported quantity (scalar or vectorial)
κ	Indicator function
η	Dynamic viscosity, [Pa·s]
μ	Mass loading, [kg/kg]
μ_{pp}	Inter-particle friction coefficient
ρ	Mass density, [kg/m^3]
τ	Characteristic time scale, [s]
$\boldsymbol{\tau}$	Stress, [Pa]
$\boldsymbol{\Phi}$	Volumetric coupling force, [N/m³]

Latin Symbols

$\mathbf{a}$	Acceleration, [m/s²]
d	Diameter, [m]
e	Coefficient of restitution
$\mathbf{f}$	Force, [N]
$\mathbf{g}$	Gravity, [m/s²]
l	Length, [m]
m	Mass flow rate, [kg/s]
p	Pressure, [Pa]
t	Time, [s]
$\mathbf{u}$	Fluid velocity, [m/s]
$\mathbf{v}$	Particle velocity, [m/s]
w	Weighting function
x,y,z	Cartesian coordinate, [m]
CG	Coarse graining ratio, ($CG = d_{parcel}/d_p$)
Co	Courant number
D	Diffusion coefficient, [m²/s]
L,H,W	Channel length, height, width, [m]
N	Number of particles
S	Source term (scalar or vectorial)
U	Characteristic velocity, [m/s]
V	Volume, [m³]
X,Y,Z	Overall extension of simulation domain, [m]

Sub/superscripts

*	Dimensionless quantity
$\langle\rangle$	Domain-averaged quantity
c	Cell centered value
d	Drag
f	Fluid
i	Particle index
inlet	At the inlet
j	Fluid cell index
jet	Jet property
m	Sub-time stepping index
n	Time index
p	Particle (primary)
parcel	Parcel (computational)
s	Superficial
t	Terminal
slip	Relative between the two phases
orig	Original (unsmoothed) variable

INTRODUCTION

EL simulations are of key importance to simulate the flow in (i) gas-particle separation devices, (ii) reactive fluidized beds with changing particle properties (e.g., size, porosity, or chemical composition), or (iii) particle

classification equipment. In case the particle population is polydisperse and particles are non-spherical, EL (or hybrid EL-Euler) simulations are currently the only reliable tool to investigate cluster formation, mixing or segregation effects. However, EL simulations are computationally expensive, and this work aims on providing some guidance for selecting appropriate numerical schemes that alleviate challenges associated with the maximum allowable computation time.

One important class of numerical schemes used in EL simulations is the coupling scheme that is used to transfer information from the particle phase to the Eulerian phase (i.e., "two-way" or "back-coupling"). For the coupling scheme a variety of strategies are available in literature. For example, the group of Sommerfeld (Lain and Sommerfeld, 2008; Sommerfeld and Lain, 2012) used an under-relaxation technique in which particle-phase properties are pre-averaged (in time) before the back-coupling is performed. Despite the great success of this technique in predicting experimental data, this approach cannot be used for a time-resolved simulation, and also cannot strictly guarantee Newton's Third Law (i.e., "action et reactio") in an instantaneous sense. Another approach (called "EUgran+poly") has been chosen by the group of Pirker (Schellander et al., 2013), in which a transient simulation (based on an Euler-Euler approach and a mean particle diameter of the particle cloud) is performed first. Then, tracer particles are used to predict individual particle trajectories in a polydisperse particulate flow. Finally, the mean particle diameter of the granular (Euler) phase is updated, and the transient Euler-Euler simulation is continued. While both strategies have proven to be very efficient in terms of computation time, they are not fully transient in the sense that both phases are updated in a time-resolved fashion. Furthermore, these two approaches are limited to moderately dense flows, because their collision models rely on closures from kinetic theory.

In this work we focus on a fully transient approach, which is based on the classical CFD-DEM (Zhou et al., 2010). This approach allows simulations of fluid-particulate flows from the dilute to very dense regimes (i.e., near or above the close-packing limit), which is its key advantage. Specifically, we have chosen the implementation CFDEMcoupling (www.cfdem.com) as the basis of our work, which relies on a parallel implementation of a finite-volume fluid solver (N.N., 2013), and the DEM (Kloss et al., 2012).

In the next chapter we briefly explain the underlying model equations, and the coupling algorithms we have implemented in CFDEMcoupling. We then analyse the time-step restrictions immanent to phase coupling, and finally consider a variety of test cases in order to benchmark the coupling algorithms. By considering a wide range of numerical parameters, we highlight the effect of these parameters on the predictions and the implications in terms of the computation time step required to ensure a stable integration. This allows us to give recommendations for numerical parameters that yield predictions with acceptable accuracy at a minimal computational cost.

MODEL DESCRIPTION

CFD-DEM Approach

The well-known CFD-DEM approach (Zhou et al., 2010) relies on the solution of the filtered Navier-Stokes equations, i.e.,

$$\frac{\partial\left(\rho_f \phi_f\right)}{\partial t} + \nabla\cdot\left(\rho_f \phi_f \mathbf{u}\right) = 0\,, \qquad (1)$$

$$\frac{\partial\left(\rho_f \phi_f \mathbf{u}\right)}{\partial \mathrm{t}} + \nabla\cdot\left(\rho_f \phi_f \mathbf{u}\mathbf{u}\right) = -\phi_f \nabla p_f - \phi_f \nabla\cdot\boldsymbol{\tau}_f + \boldsymbol{\Phi}_d + \rho_f \phi_f \mathbf{g}\,, \qquad (2)$$

and the integration of Newton's equation of (translational and rotational) motion for each individual particle. Here $\boldsymbol{\Phi}_d$ is a volumetric coupling force (excluding buoyancy effects), i.e., the force exerted by the particle phase on the fluid phase per unit volume of the gas-particle mixture.

Assuming a fixed particle mass, Newton's equation of translational motion yields an equation for the acceleration of each individual particle. Taking into account (i) contact, (ii) drag, (iii) fluid-stress, and (iv) gravitational forces, this equation is:

$$\mathbf{a}_i = \frac{\mathbf{f}_{cont,i}}{\rho_p V_{p,i}} + \frac{\beta_{p,i}}{\rho_p}\left(\mathbf{u}_i - \mathbf{v}_i\right) - \frac{1}{\rho_p}\nabla\cdot\boldsymbol{\tau}_f + \mathbf{g}\cdot \qquad (3)$$

The integration of the above equations is straight forward once each force component has been computed based on particle and fluid data available at time t^m and t^n, respectively. Note, that in this work we have considered only contact forces to integrate the equations of rotational motion, and have neglected hydrodynamic torque.

The above equation requires closures for the contact forces, the fluid-particle friction coefficient, and the fluid stress. We use a standard linear spring-dashpot model for the contact forces, the model proposed by Beetstra et al. (2010) for the friction coefficient, and a laminar fluid stress model.

CFD-DPM Approach

In order to simulate systems of industrial scale, the CFD-DEM approach cannot be used because of the excessively large number of (physical) particles. Instead, various flavours of "parcel methods", in which computational parcels are used to represent multiple physical particles, have been documented in literature during the last fifteen years. In CFDEMcoupling, both the MP-PIC method introduced by Snider (2001), as well as the DPM approach by Patankar and Joseph (2001) is available. While the MP-PIC approach does not require direct tracking of (parcel) collisions, DPM relies on a detection of collisions of spheres that represent a typical collision volume of each parcel. In parcel-based approaches, fluid-particle interaction forces are based on the physical diameter of the particles that are represented by each parcel. In such a way, fluid-particle momentum transfer can be modelled correctly.

We find that for situations involving dense granular flows the DPM results in much more robust simulation compared to the MP-PIC method. Consequently, we

have used the DPM approach in all the simulations presented in this paper.

Coupling Algorithm

The overall flow chart for the coupling algorithm implemented in CFDEMcoupling is illustrated in Figure 1. Starting with the known fluid and particle velocities, Eulerian quantities (e.g., the fluid velocity, or the voidage) are interpolated at the particle location to allow the computation of forces acting on each particle. Particle properties (i.e., velocity and position) are then updated with sub-time stepping (time index m), either in an implicit or an explicit fashion. Note, that for implicit time marching of the particles, the fluid velocity at the particle position and the drag coefficient must be known. In this work, we have used explicit time marching for the particle phase.

Updating the fluid flow field is more involved, and is detailed in the following paragraphs.

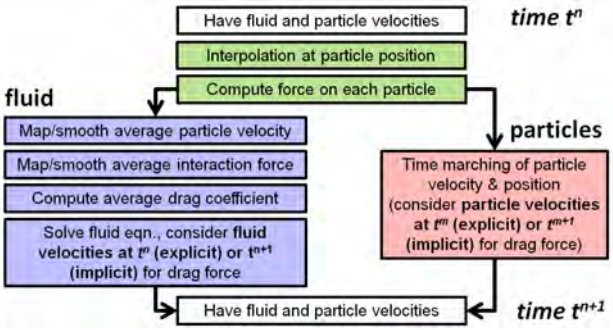

Figure 1: Flow chart of the coupling algorithm.

Mapping Algorithm

A mapping algorithm is used to calculate the weights w_{ij} that determine the contribution of the properties of particle i to cell j. The algorithm used in this work is based on a simple search algorithm that uses 29 satellite points (located inside the particle or parcel volume). Specifically, w_{ij} is determined by the number of satellite points of particle i that are located in cell j, divided by the total number of satellite points (of particle i) that are located in the fluid domain. This simple algorithm is very robust, conserves particle properties, can be used for any polyhedral mesh, and naturally handles situations in which particles are located near walls. Note that each particle (or parcel) only contributes to cells which are physically overlapping with the particle. This situation is unsatisfactory in case the typical size of a fluid cell is in the order of, or smaller than the particle (or parcel) diameter. In the following, we discuss an approach to overcome this limitation.

Smoothing

After the mapping algorithm has been executed, filtered Eulerian quantities (with a filter length equal to the grid spacing Δx) of the particle properties are available at the fluid grid. These quantities can now be smoothed over a length l_{smooth}. The physical meaning of this smoothing length is that each particle (or parcel in case of the DPM) will influence the fluid around it over a certain distance. Naturally, this distance will be some multiple of the particle (or parcel) radius. Typically, we have chosen $l_{smooth} = 3d_p$ in this work. Note that such a smoothing procedure is only relevant for small $\Delta x/d_p$ ratios. In case this ratio is large, however, the smoothing inherent to the mapping algorithm yields satisfactory exchange fields, and smoothing has no effect.

The smoothing operation is realized by (implicit) solution of a diffusion equation for each transferred quantity γ (e.g., the coupling force $\mathbf{\Phi}$):

$$\frac{\partial \gamma}{\partial t} = D\nabla^2\gamma \,. \qquad (4)$$

Here the diffusion coefficient is computed as $D = l_{smooth}^2/\Delta t$. Note that this smoothing operation is conservative, and has been used in previous work (Capecelatro and Desjardins, 2013; Pirker et al., 2011).

In case an implicit time marching for the fluid phase is used (see next section), a smoothed mean particle velocity field must be available. When performing the smoothing operation, the mean particle velocity field must be fixed in cells where particles are present ("filled cells"), and smoothing must be applied only to neighbour cells (of these filled cells). This can be realized by adding a source term S in the diffusion equation, i.e.,

$$S_\alpha = \frac{\kappa}{\Delta t}\left(\gamma_{orig} - \gamma\right), \text{ with}$$
$$\kappa = \begin{cases} 10^5 \;\; if\, \gamma_{orig} \neq 0 \\ 0 \;\; otherwise \end{cases}, \qquad (5)$$

that forces the original values (γ_{orig}) in filled cells to remain unchanged during the smoothing operation (Pirker et al., 2011).

Implicit/Explicit Time Marching for the Fluid Phase

At this point it is important to note that the volumetric coupling force $\mathbf{\Phi}$ can dominate Eqn. 2 in dense gas-particle flows involving small (i.e., d_p < ca. 100 µm) particles. In such a situation, this term is balanced (to a first approximation) with the pressure gradient term (i.e., the first term on the right hand side of Eqn. 2). Consequently, an implicit treatment of the coupling force $\mathbf{\Phi}$ would be desirable when updating the fluid's velocity and pressure field, because it would improve the stability of the integration. Indeed, we find that an implicit handling allows us to take 5 to 15 times larger fluid time steps, critically reducing the computation time in situations in which the load from the fluid solver is substantial compared to the particle solver.

In most gas-particulate flows, the drag force is the key force component, hence $\mathbf{\Phi} \approx \mathbf{\Phi}_d$. $\mathbf{\Phi}_d$ is a function of the local fluid and particle velocity, as well as the fluid-particle friction coefficient β experienced by each individual particle. The total coupling force available at the new time t^{n+1} (but before updating the fluid velocity) is:

$$\mathbf{\Phi}_{d,j}{}^{n+1} = -\frac{1}{V_j}\sum_i w_{ij} V_{p,i} \beta_{p,i} \left(\mathbf{u}_i{}^n - \mathbf{v}_i{}^{n+1}\right) \qquad (6)$$

Note that it is not possible to consider the new fluid velocity $\mathbf{u}_i{}^{n+1}$ in the calculation of the total coupling force given by Eqn. 6, since particle velocities are advanced with sub-time stepping. To realize an implicit coupling, i.e., consider the new fluid velocity $\mathbf{u}_c{}^{n+1}$ (located at the cell centres), it is necessary to recast the coupling force in an expression that involves an average

fluid-particle friction coefficient, as well as an average relative particle velocity. Thus,

$$\mathbf{\Phi}_{d,j}^{\,n+1} = -\frac{\left\langle w_{ij} V_{p,i} \beta_{p,i} \right\rangle}{V_j} \left(\mathbf{u}_c^{\,n} - \left\langle \mathbf{v}_i^{\,n+1} \right\rangle \right). \qquad (7)$$

One can now easily calculate the average friction coefficient $<w_{ij}V_{p,i}\beta_{p,i}>$ from Eqn. 7 based on (the known) value for $\mathbf{\Phi}_d$. In case an implicit handling of the coupling force is performed, the new fluid velocity appears in the expression for the coupling force, leading to a slightly different version of Eqn. 7:

$$\mathbf{\Phi}_{d,j}^{\,n+1'} = -\frac{\left\langle w_{ij} V_{p,i} \beta_{p,i} \right\rangle}{V_j} \left(\mathbf{u}_c^{\,n+1} - \left\langle \mathbf{v}_i^{\,n+1} \right\rangle \right). \qquad (8)$$

Note, that such an implicit handling of the coupling force has two important consequences: (i) Newton's Third Law is not strictly enforced (because $\mathbf{\Phi}_{d,j}^{\,n+1} \neq \mathbf{\Phi}_{d,j}^{\,n+1'}$), and (ii) the effect of particle velocity fluctuations (which might affect $\beta_{p,i}$) is not accounted for. While the latter is thought to be of minor importance for typical gas-particle flows involving particles with d_p < 100 µm, the former is of concern in case an exact conservation of the system's momentum is required. We will discuss this point in our results for the freely sedimenting suspensions.

The interested reader might have observed another subtle difference between Eqns. 6, 7 and 8: particle-based quantities (index *i*) have been replaced by cell-based quantities (index *c*) when solving the fluid's governing equations. This is a problem when using an implicit scheme, i.e., one employs Eqn. 8, because the drag force on a particle is related to $\mathbf{u}_i$ and $\mathbf{v}_i$ (and not $\mathbf{u}_c$ and $\langle \mathbf{v}_i \rangle$). We have previously proposed a force splitting scheme (see Radl et al., 2012) that accounts for this discrepancy by splitting-off an explicit force component. Tests show that in dense flows (e.g., packed beds) this splitting increases the stability of the fluid solver (data not shown). We have indicated results obtained by such an improved method by "split impl./expl." in the current work. Furthermore, we have considered a variant of the coupling algorithm in which we treat the coupling force in cells that are void of particles (and hence no average particle velocity can be estimated) explicitly. In the remaining fluid cells the coupling force was treated implicitly. Such an approach avoids the need for smoothing the (average) particle velocity field, which we find to be problematic in regions with high particle velocity gradients.

THEORETICAL CONSIDERATIONS

Relaxation Times

A key physical time scale in a gas-particle flow is the particle relaxation time τ_p defined as (assuming Stokes drag law):

$$\tau_p = \frac{d_p^{\,2} \rho_p}{18 \eta_f}. \qquad (9)$$

This time scale sets an upper bound for the numerical integration of the particles' equation of motion (note that the particle-particle interaction force model might impose an additional limitation on the time step). Physically, this time scale can be interpreted as the time needed to accelerate the particle to a certain fluid velocity *U* by means of drag forces. The time step used for the integration of the particle equations must be smaller than the particle relaxation time in order to ensure an accurate and stable (in case of a simple forward Euler integration) numerical simulation.

Similarly, one can define a fluid relaxation time τ_f as:

$$\tau_f = \frac{U}{a_f} = \frac{\tau_p}{\mu} = \frac{d_p^{\,2} \rho_f}{18 \eta_f} \frac{1-\phi_p}{\phi_p}. \qquad (10)$$

Here a_f is a typical acceleration of the fluid due to drag forces. This time scale can be interpreted as the time it takes for the fluid to accelerate to a certain particle velocity *U* under the action of drag forces. This time scale sets an upper bound for the numerical integration of the equations that govern fluid flow. Clearly, the time step used for the integration of the Navier-Stokes equations must be smaller than the fluid relaxation time. In typical gas-particle flows with moderate to large particle volume fractions, and particles in the µm size-range, this fluid relaxation time is $O(10^{-5})$ seconds or smaller, depending on the mass loading.

Time Step Restrictions

In addition to the above characteristic relaxation times, the Courant number *Co* must be kept sufficiently low (typically less than 0.5) in order to ensure a stable numerical solution. Thus, the characteristic time scale

$$\tau_{Co} = \frac{\Delta x}{U} Co \qquad (11)$$

limits the fluid time step.

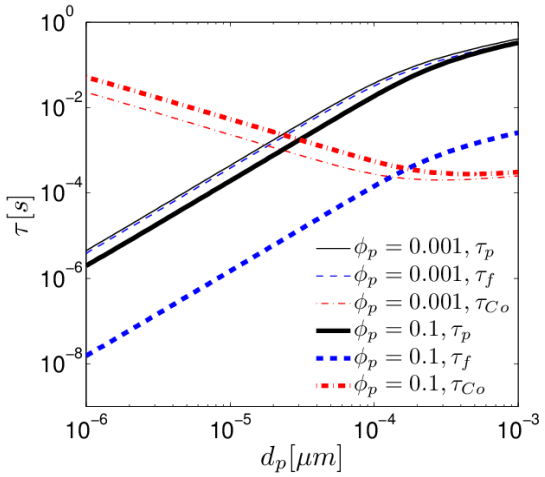

Figure 2: Characteristic time scales relevant for the simulation of a freely-sedimenting gas-particle suspension (ρ_p = 1500 [kg/m³], $\eta_f = 1.8 \cdot 10^{-5}$ [Pa·s], ρ_f = 1.3 [kg/m³], Beetstra et al. drag law).

The time step restrictions for integrating the Navier-Stokes equations are summarized in Figure 2 for a freely sedimenting gas-particle suspension. Note that in this figure the particle and fluid relaxation time for dense suspensions at non-zero Reynolds numbers have been computed using the drag model of Beetstra et al. (2010). As can be seen, for a dilute suspension (i.e., ϕ_p = 0.001), the particle relaxation time becomes the limiting time scale in case particles are smaller than ca. 15 µm, and τ_f

$\approx \tau_p$. However, for moderately dense suspensions (i.e., $\phi_p = 0.1$) the largest possible time step is set by the fluid relaxation time τ_f for particle diameters smaller than ca. 200 µm. For particles with a diameter of ca. 20 µm or smaller, the largest possible time step becomes $O(10^{-6})$ seconds or smaller. Thus, an integration of the Navier-Stokes equations for these systems requires very small time steps, or a robust (implicit) coupling algorithm, such as the one we have outlined above.

RESULTS

Bi-Disperse Bubbling Fluidized Bed (CFD-DEM)

To illustrate that our proposed methodology can handle systems near close packing, we have simulated the bubbling fluidized originally studied by Goldschmidt et al. (2003), and simulated recently by Capecelatro and Desjardins (2013). Key system parameters are summarized in Table 1. In these simulations an implicit time marching for the fluid phase was performed, and no smoothing of exchange fields was performed.

Predictions both from the current work and from literature are summarized in Figure 3. As can be seen, there is reasonable agreement in the predicted particle distribution. However, the shape of the interface between the two particle species is different, especially for longer simulation times. A possible explanation of this difference is the different drag law used in the simulations. Specifically, our comparison of particle velocities (see Figure 4) might hint to differences in the particle flow pattern caused by bubbling. Unfortunately, we could not find reference results for the particle flow pattern in literature. Hence, we can only speculate about the effect of bubbling, and have included snapshots of the particle velocity distribution in Figure 4.

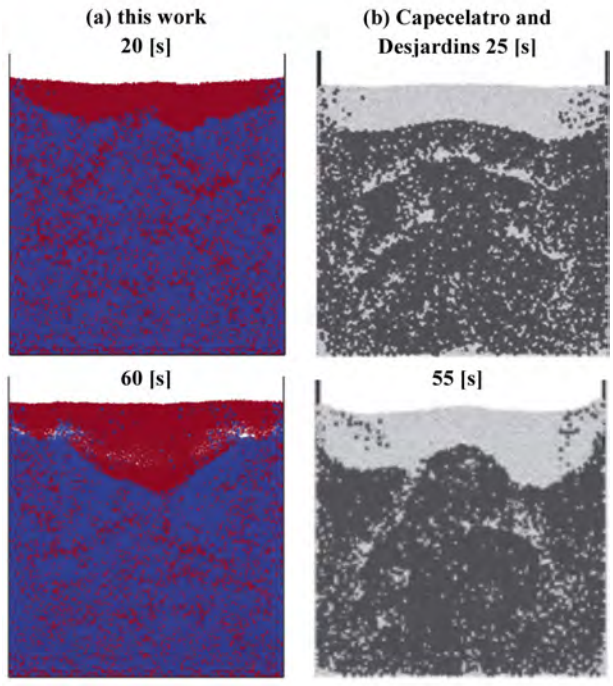

Figure 3: Snapshots of the spatial distribution of particles in a bubbling fluidized bed (a: this work, small particles are colored red and large particles are colored blue; b: literature data from Capecelatro and Desjardins, 2013, using the Tenneti et al., 2011, drag model).

Our results indicate that there is noticeable particle motion only near the free interface of the particle bed, and distinct bubbles do not form. Also, we found that even for moderate diameter ratios (i.e., 1.67 as in the current presentation), the drag formulation had a significant impact on the predicted bed expansion (i.e., bubbles occurred for other drag models) and on the segregation profile. Surprisingly, we found that the standard (i.e., mono-disperse) formulation of the drag model provided by Beetstra et al. (2010) gave the best agreement with the experimental data of Goldschmidt et al. (2003). Interestingly, also Capecelatro and Desjardins (2013) used a drag law that has been designed for mono-disperse particle beds. Thus, more research is needed to explain why a mono-disperse drag formulation gives better predictions for bi-disperse bubbling bed compared to more elaborate drag models.

Table 1: Physical parameters of the bubbling fluidized bed test case.

Parameter	*Value*
Domain (X x Y x Z)	0.15 x 0.015 x 0.45 [m]
Particle density (ρ_p)	2525 [kg/m³]
Particle diameter (d_p)	1.5 … 2.5 [mm]
Gas density (ρ_f)	1.13 [kg/m³]
Gas dynamic viscosity (η_f)	$1.77 \cdot 10^{-5}$ [Pa·s]
$N_{p,1}$ / $N_{p,2}$	17,940 / 27,720
U_s	1.3 [m/s]
e_p / μ_{pp}	0.9 / 0.1

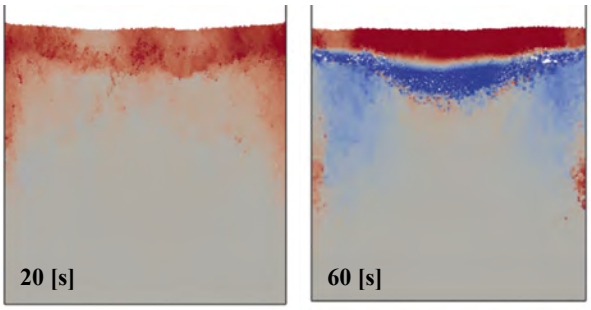

Figure 4: Snapshots of the vertical (i.e., z-) particle velocity in a bubbling fluidized bed (colors indicate velocities between -0.06, blue, and +0.06 [m/s], red, t = 60 [s]).

Freely Sedimenting Suspension (CFD-DPM)

A critical test for an EL code is its ability to predict the fluid-particle slip velocity during the sedimentation in a fully periodic box. In such a configuration no external forces act on the fluid-particle system (the weight of the system must be balanced by pressure gradient, though). Hence the total momentum of the system should remain unchanged. We have performed simulations of a sedimenting gas-particle mixture (d_p = 150 µm, ρ_p = 1500 kg/m³, $\langle\phi_p\rangle$ = 0.10, the gas phase was air at ambient conditions) using implicit and explicit time marching for the fluid phase. Results for the domain-averaged slip velocity (i.e., the difference between the momentum-averaged velocity of the two phases) for several choices of the dimensionless fluid time step Δt^*

= $\Delta t/t_f$ are summarized in Figure 5. Our simulations using an explicit time marching were performed with a time step of Δt^*=0.025 - larger simulations were impossible due to stability reasons. As can be seen, the results of the implicit time marching are in good agreement with the results for the explicit procedure (fluid grid size effects are typically larger, see blue and black symbols in Figure 5; note that these fluid grid size effects arise naturally due to non-resolved fluid velocity fluctuations, see Radl et al., 2012). The advantage of the implicit procedure is that it allows a time step up to 17.5 times larger than the one used for an explicit procedure.
As mentioned in the previous chapter, an implicit procedure does not perfectly enforce Newton's Third Law, and hence leads to a drift of the system's momentum. In order to control the drift velocity, it is necessary to add a correction force that is in the order of 5 to 15% of the total system weight (the correction in case of the explicit procedure is much smaller, i.e., 0.4%; splitting the coupling force into an implicit and explicit part reduces the necessary correction force to ca. 1% of the system weight). This correction force reflects the integral error due to the violation of Newton's Third Law. Furthermore, we find that the correction force depends on the fluid grid size (smaller grid size lead to a smaller correction), i.e., the correction is proportional to the number of particles per fluid grid cell. In summary, one should carefully evaluate whether implicit time marching yields accurate results, especially in case comparably coarse fluid grid cells are used. Our simulation results indicate that this is typically the case for moderately dense to dense gas-particle suspensions. In dilute flows (for which τ_f is close to, or larger than τ_p), we suggest using an explicit procedure, or an algorithm based on implicit/explicit force splitting because of a more precise conservation of the system's momentum.

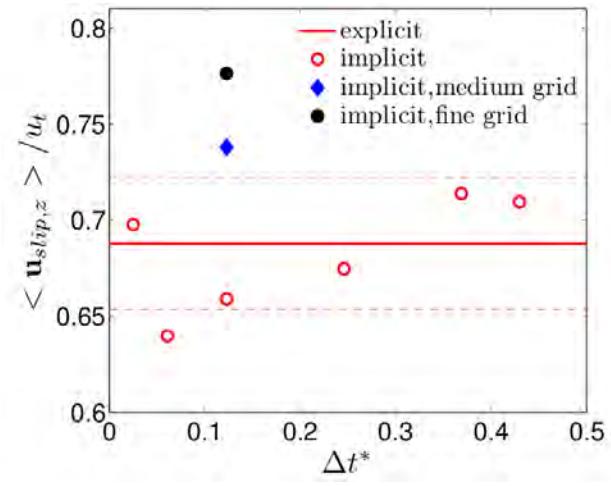

Figure 5: Predicted slip velocity of a freely-sedimenting gas-particle suspension for various dimensionless fluid time steps (the red dashed lines indicate ± 5% of the results using the explicit coupling procedure).

2D Bi-Disperse Jet in Cross Flow (CFD-DPM)

Setup

To investigate the performance of the mapping and smoothing schemes to model comparably dilute flows, we consider the injection of a particle jet in a turbulent cross flow (JICF). Specifically, we consider a synthetic configuration, in which a bi-disperse particle population is injected into a (pseudo) two-dimensional fluid flow field (i.e., air at ambient conditions). The physical parameters of the JICF configuration are summarized in Table 2. The fluid mesh resolution was Δx = 0.01 [m], and the time resolution of the base case was $\Delta t = 10^{-5}$ [s] to advance the fluid's governing equations.

Table 2: Physical parameters of the 2D JICF test case.

Parameter	*Value*
Domain (X x Y x Z)	1.8 x 0.7 x 0.002 [m]
Particle density (ρ_p)	2500 [kg/m³]
Particle diameter (d_p)	5 … 20 [µm]
Gas density (ρ_f)	1.1 [kg/m³]
Gas dynamic viscosity (η_f)	$1.91 \cdot 10^{-5}$ [Pa·s]
Mass loading ($\mu = m_p/m_f$)	0.5
Rel. particle injection velocity ($\mathbf{v}_y/\mathbf{u}_{inlet,x}$)	0.591
Crossflow velocity ($\mathbf{u}_{inlet,x}$)	25.4 [m/s]

Particle Penetration

Maps of the time-averaged magnitude of the gas velocity, as well as the particle positions are shown in Figure 6. Again, we have attempted to assess the effect of an implicit vs. an explicit time marching procedure on key flow features. As can be seen, explicit time marching leads to a more pronounced particle penetration into the cross flow compared to the implicit procedure (cp. Figure 6a and b). However, the recirculation behind the injection point has a similar extension in the main flow direction whether the implicit or the explicit procedure is employed. The advantage of implicit time marching is that we were able to use a substantially (i.e., 4.9 times) larger time step. Such a large time step could not be realized with explicit time marching, highlighting the robustness of the implicit procedure. Furthermore, we show results for the implicit/explicit coupling force splitting in Figure 6c (in Figure 7 the splitting of the coupling force is illustrated). As we will show in the next paragraph, this force splitting approach yields results that are practically indistinguishable from that obtained with an explicit procedure, but require less computational resources.

Velocity Profiles

A more quantitative comparison of the 2D JICF results is provided in Figure 8, where we have plotted profiles of the time-averaged streamwise (i.e., x-) fluid velocity component. As can be seen, the results for various flavours of the implicit time marching are essentially indistinguishable from each other. Same as for the particle penetration illustrated in Figure 6, the explicit procedure leads almost identical predictions for the velocity distribution when compared to the implicit/explicit mapping approaches. For the time being, we accept our results obtained with the explicit

and implicit/explicit mapping approach as the most accurate predictions (in these simulations Newton's third law is satisfied with an error of less than 1%; experimental validation was addressed to future work). In contrast, and as can be seen in Figure 8, a purely implicit procedure leads to an underprediction of the fluid velocity, especially near the bottom wall. Inspection of the error due to the implicit handling of the coupling force indicates that this error indeed can be substantial (data not shown). This is especially true for the uppermost layer of particles that experiences the highest acceleration, and hence also exerts the largest force onto the fluid.

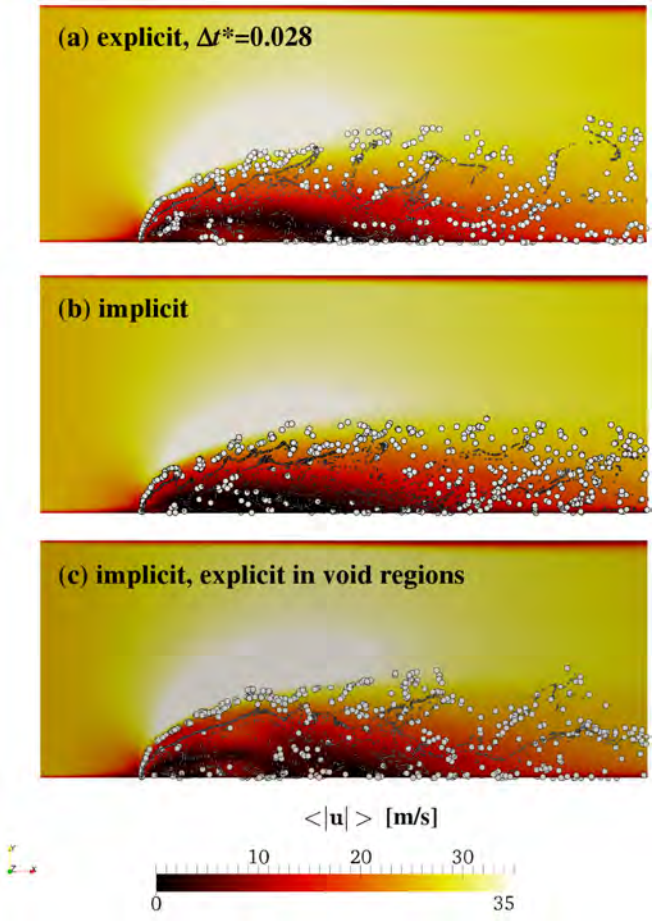

Figure 6: Time-averaged magnitude of the fluid velocity (contours), and particle distribution in the 2D JICF test case (Δt^*=0.138; the simulations in panel c employed impl./expl. force splitting; smoothing based on the local particle diameter was applied; particles are scaled according their primary particle diameter).

Finally, we note that whether smoothing is employed or not results in minimal differences in the predicted flow pattern. This is because of the comparably large fluid grid to parcel diameter ratio that results in a sufficient smoothing inherent to the grid size.

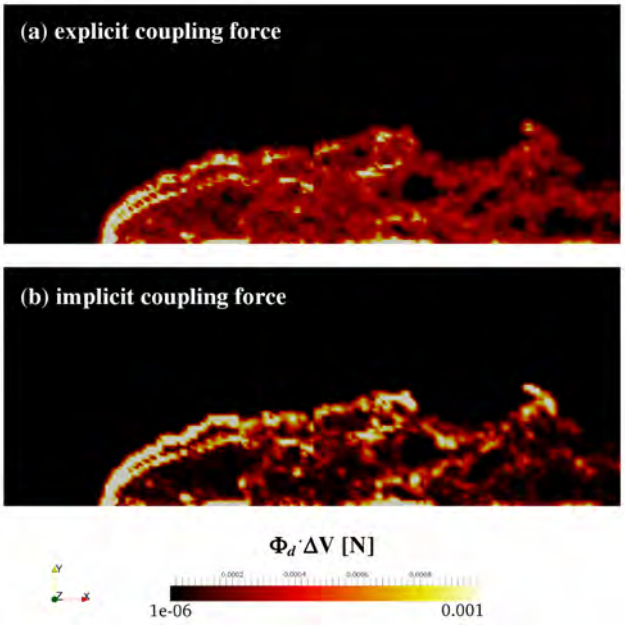

Figure 7: Local coupling force obtained from simulations with implicit force coupling in dense regions, and explicit force treatment in regions void of particles (data from Figure 6c; impl./expl. force splitting was performed).

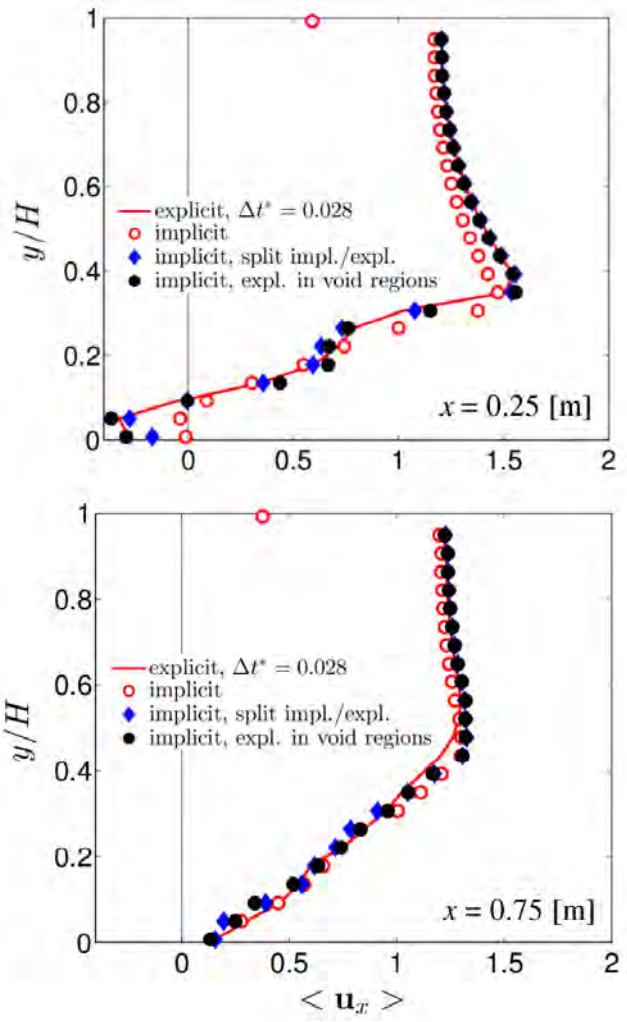

Figure 8: Sensitivity of the fluid velocity profiles in the JICF configuration to the coupling procedure and the fluid time step.

The Salzman 3D JICF Configuration (CFD-DPM)

To investigate whether the developed coupling algorithm can give results independent of parcel size and fluid grid resolution, the (three-dimensional) JICF configuration of Salzman and Schwarz was simulated. The physical parameters are summarized in Table 3, and the geometrical details are shown in Figure 9.

The Salzman configuration has been analysed numerically by Li and Lin (2010), as well as Han and Chung (1992). Only a limited amount of reliable reference data is available for this setup. Therefore, in this work we have used a highly-resolved CFD-DPM simulation with approximately 12.7 Mio. fluid cells to provide reference data for the subsequent analysis. A sub-grid-scale stress model for unresolved fluid velocity fluctuations has been used in this reference simulation. Analysis of the resolved and sub-grid-scale velocity fluctuations indicate that the former are roughly three times larger than the latter downstream of the injection point. Thus, we conclude that sub-grid scale (fluid) velocity do not play an essential role for this reference simulation.

Table 3: Physical parameters of the Salzman JICF test case.

Parameter	*Value*
Jet Diameter (d_{jet})	4.62 [mm]
Particle density (ρ_p)	2638 [kg/m³]
Particle diameter (d_p)	15 [µm]
Gas density (ρ_f)	1.1 [kg/m³]
Gas dynamic viscosity (η_f)	$1.91 \cdot 10^{-5}$ [Pa·s]
Jet mass loading ($m_p/m_{f,jet}$)	20.8
Rel. particle injection velocity ($\mathbf{v}_y/\mathbf{u}_y)_{jet}$	1
Rel. jet velocity ($\mathbf{u}_y/\ \mathbf{u}_{inlet,x}$)	1.57
Crossflow velocity ($\mathbf{u}_{inlet,x}$)	16.8 [m/s]

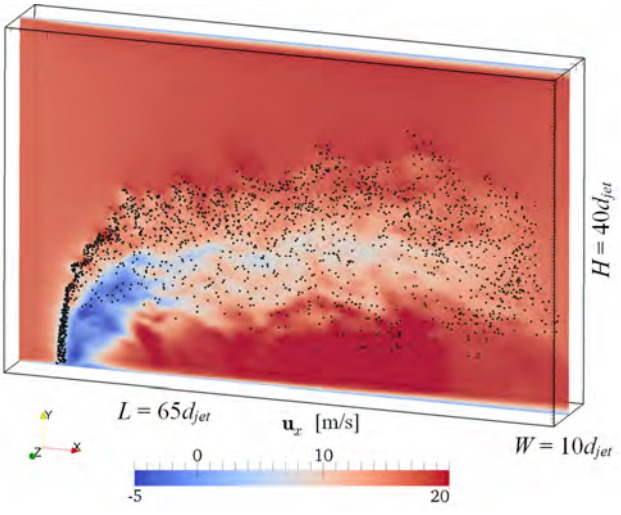

Figure 9: Instantaneous *x*-component of the fluid velocity (contours are shown in a central cut plane), and particle distribution (black dots) in the Salzman JICF configuration.

Particle Penetration

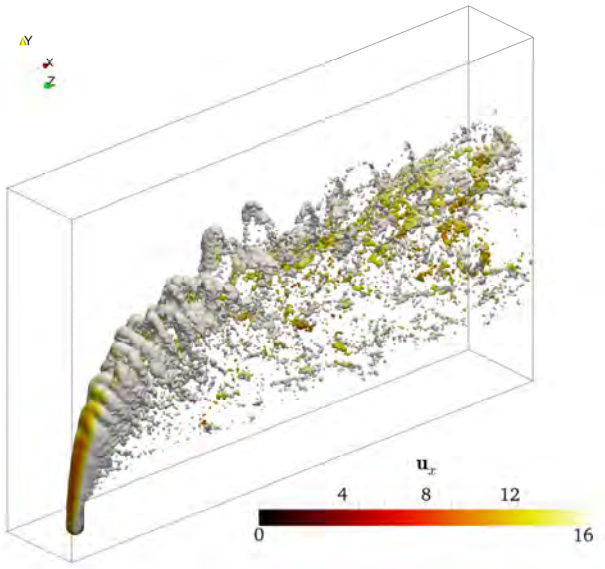

Figure 10: Instantaneous fluid velocity distribution (in [m/s]) on an iso-surface of the particle volume fraction ($\phi_p = 3.5.10^{-4}$) for the Salzman JICF configuration (reference simulation with *CG* = 5, 510 x 314 x 79 grid cells).

Figure 10 and Figure 11 summarize the results for the particle dispersion pattern, as well as the effect of the fluid grid resolution and the coarse graining ratio (*CG*) on our predictions. The reference simulation (see Figure 10) highlights that a complex three-dimensional flow structure develops downstream of the particle injection point. The particle concentration is highest in a U-shaped region that becomes more and more diffuse in the streamwise (i.e., *x*-) direction. Interestingly, the reference simulation predicts a region of comparably low fluid velocity inside this U-shaped region.

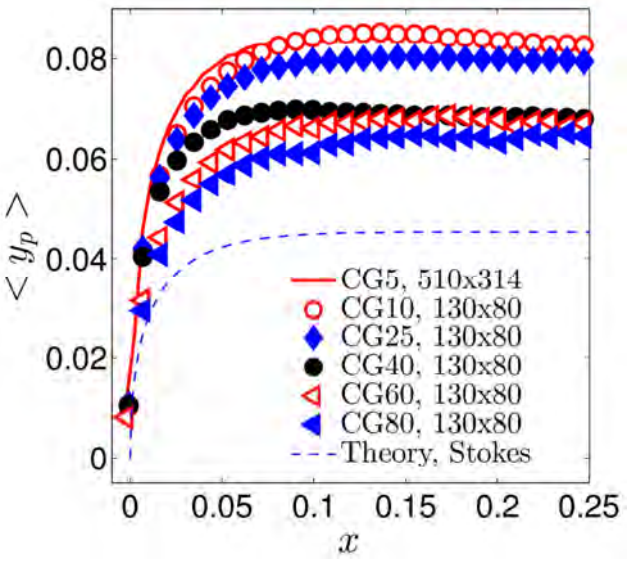

Figure 11: Mean vertical particle position as a function of the streamwise (i.e., *x*-) position to quantify the penetration of the particle jet into the cross flow (dimensions in [m]; all simulations used the smoothing algorithm).

By computing the centre of mass position of the particle population as a function of the streamwise position, we quantify the effect of various numerical settings on the predicted gas-particle flow (see Figure 11). As can be seen, all results with *CG* = 25 (or smaller), show

reasonable agreement with the reference results. For these simulations the smoothing procedure as well as the details of the coupling algorithm had a comparably small effect on the particles' mean trajectory. Results with CG = 40 (or larger) give less satisfactory results, and not employing the smoothing algorithm for CG = 40 (or larger) gave the worst predictions (data not shown). Also, we find that increasing the smoothing length does not improve the predictions for CG = 40 or larger (data not shown). The physical reason for this limitation is the inability to resolve particle and fluid velocity fluctuations when employing extremely large CG ratios. This indicates that (for large parcel sizes) the introduction of a smoothing step can improve the quality of predictions, however, the predictive capabilities are limited by clustering effects not accounted for by the models used by us.

We would like to note that smoothing introduces only an incremental computational cost. Specifically, our simulations indicate that smoothing introduces an additional computational overhead of ca. 18%, but substantially improves the predictions as discussed above.

In summary, we observe that for excessively large CG ratios the jet penetration is underestimated, i.e., a too small disturbance of the flow is predicted. In Figure 11 (blue dashed line) we have also included the theoretical trajectory of an injected particle under the assumption of (i) an undisturbed background flow, as well as (ii) the validity of Stokes' drag relation. As can be seen, all our simulations predict a penetration of the particle jet into the cross flow that is ca. 1.5 to 2 times larger than this theoretical result.

CONCLUSION

We have presented details of numerical schemes implemented in the open-source package CFDEMcoupling, which are relevant for the robust simulation of gas-particle flows involving broad particle size distributions. We made an attempt to estimate relevant time scales that limit the time step in these simulations. We then critically analysed the effect of an implicit time marching procedure for various test cases. Based on our results for a freely sedimenting gas-particle suspension, we conclude that the proposed implicit integration procedure is not strictly conservative, and gives an error between 5% and 15 % depending on the number of particles per computational cell. An improved coupling algorithm that splits the force into an explicit and implicit contribution can alleviate this problem. Clearly, an implicit procedure is essential for a robust simulation in case very small particles need to be modelled. Typically, a time step ca. 15 times larger than that required for an explicit procedure can be used in case an implicit, or a hybrid implicit/explicit procedure is employed.

From our results of the jet-in-cross flow configuration, we conclude that:

1. The implicit integration procedure leads to less particle penetration into the cross flow compared to an explicit procedure. An improved algorithm that splits the coupling force into an implicit and explicit part improves the predictions.
2. Smoothing is key for the correct prediction of particle penetration into the cross flow for the 3D JICF configuration in case large CG ratios must be used. Thus, smoothing becomes essential for CG > 40, which is typically required to simulate industrial-scale problems.
3. A coarse graining ratio of 25 still gives accurate results for the 3D gas-particle JICF configuration with 15 µm primary particles.

Future work might focus on the experimental validation of our JICF simulations to confirm our conclusions.

ACKNOWLEDGEMENTS

The help of Dipl.-Ing. BSc. Stefan Darmann (TU Graz) in setting up the 2D JICF configuration is greatly acknowledged. We acknowledge the support of NAWI Graz by providing access to dcluster.tugraz.at.

REFERENCES

BEETSTRA, R., VAN DER HOEF, M.A., and KUIPERS, J.A.M., (2010), "Drag Force of Intermediate Reynolds Number Flow Past Mono- and Bidisperse Arrays of Spheres", *AIChE J.*, **53,** 489-501.

CAPECELATRO, J., and DESJARDINS, O., (2013), "An Euler–Lagrange Strategy for Simulating Particle-Laden Flows", *J. Comput. Phys.*, **238,** 1-31.

GOLDMISCHDT, M.J.V., LINK, J.M., MELLEMA, S., and KUIPERS, J.A.M., (2003), "Digital image analysis measurements of bed expansion and segregation dynamics in dense gas-fluidised beds", *Powder Technol.*, **138,** 135-159.

HAN, K.S., and CHUNG, M.K., (1992), "Numerical Simulation of Two-Phase Gas-Particle Jet in a Crossflow", *Aerosol Sci. Technol.*, **16**, 126-139.

KLOSS, C., GONIVA, C., HAGER, A., AMBERGER, S., and PIRKER, S., (2012), "Models, Algorithms and Validation for OpenSource DEM and CFD-DEM", *Progr. Comput. Fluid Dyn.*, **12,** 140-152.

LAIN, S. and SOMMERFELD, M., (2008), "Euler/Lagrange computations of pneumatic conveying in a horizontal channel with different wall roughness", *Powder Technol.*, **184,** 76-88.

LI, G., and LIN, J., (2010), "Characteristics of Particle Dispersion in a Jet in Cross-Flow Based on Computational Fluid Dynamics", in: *Asia-Pacific Power and Energy Engineering Conference.*

N.N., (2010), "OpenFOAM 2.2.1 User Manual", www.opencfd.co.uk .

PATANKAR, N.A., and JOSEPH, D.D., (2001), "Modeling and numerical simulation of particulate flows by the Eulerian-Lagrangian approach", *Int. J. Multiphase Flow*, **27**, 1659-1684.

PIRKER, S., KAHRIMANOVIC, D., and GONIVA, C., (2011), "Improving the applicability of discrete phase simulations by smoothening their exchange fields", *Appl. Math. Mod.*, **35,** 2479-2488.

RADL, S., GIRARDI, M. and SUNDARESAN, S., (2012), "Effective Drag Law for Parcel-Based

Approaches - What Can We Learn from CFD-DEM?", in: *ECCOMAS 2012*.

SCHELLANDER, D., SCHNEIDERBAUER, S., and PIRKER, S., (2013), "Numerical study of dilute and dense poly-dispersed gas-solid two-phase flows using an Eulerian and Lagrangian hybrid model", *Chem. Eng. Sci.*, **95,** 107-118.

SNIDER, D.M., (2001), "An incompressible three-dimensional multiphase particle-in-cell model for dense particle flows", *J. Comput. Phys.*, **170,** 523-549.

SOMMERFELD, M., and LAIN, S., (2012), "Analysis of dilute phase pneumatic conveying through pipe systems by the Euler/Lagrange approach", in: *Ninth International Conference on CFD in the Minerals and Process Industries*.

TENNETI, S., GARG, R., and SUBRAMANIAM, S., (2011), "Drag law for monodisperse gas – solid systems using particle-resolved direct numerical simulation of flow past fixed assemblies of spheres", *J. Multiphase Flow*, **37,** 1072-1092.

ZHOU, Z.Y., KUANG, S.B., CHU, K.W., and YU, A.B., (2010), "Discrete particle simulation of particle–fluid flow: model formulations and their applicability", *J. Fluid Mech.*, **661,** 482-510.